International Journal of Agriculture and Environmental Research

ISSN: 2455-6939

Volume: 12, Issue: 03 "May-June 2026"

VEGETATION INDEX DYNAMICS (NDVI AND SAVI) IN RESPONSE TO CLIMATIC VARIATIONS IN THE SENEGALESE PEANUT BASIN (1984-2025)

[1]*François Ngor SENE, [1]Ibra FAYE, [1]Djiby YADE and [1]Babacar NDAO

[1]Université Assane SECK de Ziguinchor, Département de Géographie, Laboratoire de Géomatique et d'Environnement (LGE), BP 523, Ziguinchor, Sénégal.

*Corresponding Author

DOI: https://doi.org/10.51193/IJAER.2026.12315

Received: 02 May 2026 / Accepted: 20 May 2026 / Published: 26 Jun. 2026

ABSTRACT

The Senegalese peanut basin, located in the Sudano-Sahelian zone, experiences significant climatic variability that strongly influences vegetation dynamics and agricultural performance. This study analyses the spatiotemporal evolution of the NDVI and SAVI indices over the period 1984-2025, using Landsat and Sentinel-2 imagery processed through Google Earth Engine, combined with CHIRPS and TerraClimate climatic datasets. An inter-sensor harmonization procedure was applied to correct the additive bias at the Landsat/Sentinel-2 transition (2017-2022), confirming minimal residual bias (< 0.02 NDVI units). Results reveal a general upward trend in vegetation indices, structured across three phases: stagnation during persistent drought (1984-1999), progressive recovery (2000-2019), and a marked acceleration after 2020, with SAVI peaks reaching 0.55-0.60. BFAST structural break analysis confirms two statistically significant breakpoints. Seasonality is tightly coupled to the rainfall regime, with a vegetation peak in September-October. Precipitation and RAI emerge as the dominant climatic drivers (RF permutation importance $\Delta MSE \sim 9.0\times10^{-4}$ and 8.0×10^{-4}, respectively), while mean temperature exerts a moderate negative effect ($r = -0.14$). Among seven models tested (GLM, Random Forest, XGBoost, GAM, SVR, Elastic Net, and a Mean Ensemble), Random Forest delivers the best predictive performance ($R^2 = 0.323$, RMSE = 0.0487), confirming the non-linear nature of climate-vegetation relationships. Bootstrap prediction intervals (B = 200) demonstrate appropriate RF calibration with ~95% coverage. Analysis of climate-unexplained NDVI residuals reveals no significant non-climatic trend (Mann-Kendall $\tau = 0.026$, $p = 0.378$), supporting climate as the primary driver of observed dynamics. ARIMA-based projections to 2040 suggest relative NDVI stability under a baseline scenario (S1: ~0.15-0.20), with a marginal decrease under a pessimistic

ISSN: 2455-6939

Volume: 12, Issue: 03 "May-June 2026"

scenario (S2: -10% precipitation, +0.5°C per decade). SAVI proves more discriminating than NDVI in sparse vegetation areas due to its soil-background correction. These findings contribute to understanding Sahelian vegetation resilience and offer an operational framework for agroecological monitoring and sustainable land management under climate change.

Keywords: NDVI, SAVI, remote sensing, climatic variability, peanut basin, Sahel, Random Forest, BFAST, inter-sensor harmonization

1. INTRODUCTION

The West African Sahel is one of the world's regions most vulnerable to interannual climatic variability and long-term climate change (Nicholson, 2013; Dai, 2011). The Senegalese peanut basin, situated between the 400 and 900 mm isohyets, at the interface of the Sahelian and Sudano-Sahelian zones, concentrates the majority of the country's rural population and represents the principal centre of rainfed agricultural production, dominated by groundnut (Arachis hypogaea L.) and pearl millet (Pennisetum glaucum) (Faye et al., 2014; Sene et al., 2024).

Between the 1960s and 1990s, this region experienced a prolonged drought that led to a drastic reduction in vegetation cover, degradation of ferruginous tropical soils, and a deep disruption of agropastoral systems (Diouf & Lambin, 2001; Sougou et al., 2021). Since the 1990s-2000s, several studies have reported a partial recovery of vegetation, interpreted as a manifestation of the "Sahel greening" phenomenon (Herrmann et al., 2005; Fensholt et al., 2012), whose mechanisms and sustainability remain debated.

Among available remote sensing indicators, the NDVI (Normalized Difference Vegetation Index) remains the most widely used vegetation index for characterizing the density, phenology and primary productivity of vegetation (Tucker, 1979; Myneni et al., 1995). However, in Sahelian environments where bare soil occupies a significant portion of the spectral signal outside the rainy season, NDVI is subject to soil-background effects that bias interpretation. To address this limitation, Huete (1988) proposed the SAVI (Soil-Adjusted Vegetation Index), which incorporates a correction factor L = 0.5, demonstrating better robustness in sparse vegetation environments.

Few studies combine long diachronic analysis (1984-2025) with the systematic NDVI-SAVI coupling, the integration of multivariate climatic indices (SPI, SPEI, PCI, RAI), inter-sensor harmonization, uncertainty quantification, and future projection modelling. This gap fully justifies the present study, which was additionally strengthened in response to peer-review recommendations (Review Report AER072114).

The present study pursues four main objectives: (i) to analyse temporal trends in NDVI and SAVI with structural break detection (BFAST); (ii) to quantify climate-vegetation relationships using seven complementary statistical and machine learning models; (iii) to quantify model uncertainty

ISSN: 2455-6939

Volume: 12, Issue: 03 "May-June 2026"

via bootstrap prediction intervals; and (iv) to project future NDVI dynamics to 2040 under baseline and pessimistic climate scenarios.

2. MATERIALS AND METHODS

2.1 Study Area

The Senegalese peanut basin is located approximately between 13°N and 16°N latitude and 14°W and 17°W longitude, covering the administrative regions of Thiès, Diourbel, Fatick, Kaolack, Kaffrine and part of Louga (Figure 1). It extends over approximately 4.7 million hectares, corresponding to nearly 24% of the national territory. The climate is of the Sudano-Sahelian type, characterized by a long dry season (October to May) and a short rainy season (June to September), with annual precipitation ranging from 400 mm in the north to 900 mm in the south. Mean annual temperatures range between 27°C and 31°C. Dominant soils are leached ferruginous tropical soils (Dior), shallow and with low water retention capacity, along with vertisols and hydromorphic soils in lowlands (Faye et al., 2014; Sougou et al., 2021). Residual natural vegetation consists of shrub and tree savannahs dominated by Guiera senegalensis, Piliostigma reticulatum, *Cordyla pinnata* and *Faidherbia albida*, integrated in traditional agroforestry systems known as "parklands".

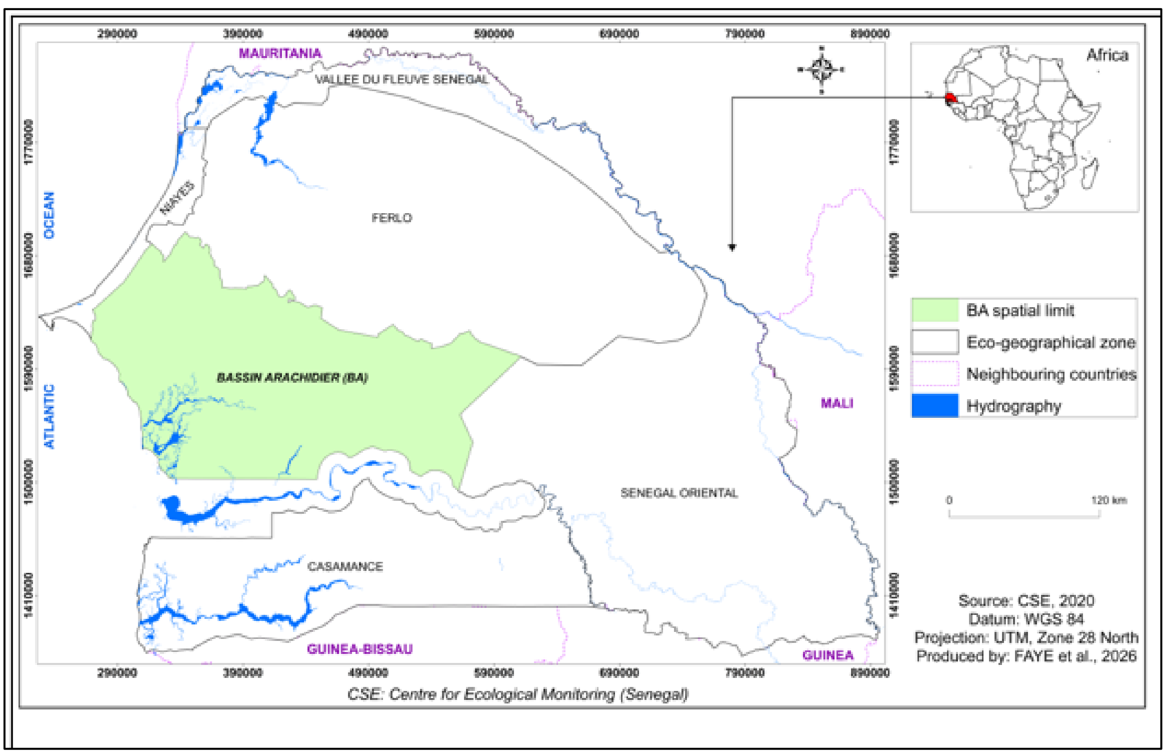

Figure 1: Location map of the study area

ISSN: 2455-6939

Volume: 12, Issue: 03 "May-June 2026"

2.2 Remote Sensing and Climatic Data

Landsat 5 TM and Landsat 7 ETM+ (Collection 2, Level-2) data were used for 1984-2021 (30 m resolution), and Sentinel-2 MSI (Level-2A) for 2022-2025 (10 m). All data were acquired and processed via Google Earth Engine. CHIRPS daily precipitation was aggregated to monthly totals; TerraClimate provided monthly minimum and maximum temperatures for computation of mean monthly temperature (TempMean). NDVI and SAVI were calculated from surface reflectance using L = 0.5 (Huete, 1988).

2.3 Inter-sensor Harmonization

To address potential inter-sensor inconsistencies between Landsat and Sentinel-2 datasets (identified as a weakness in peer review) an explicit harmonization procedure was implemented (Figure 2). The overlap period (2017-2021, when both sensor families were operational) was used to compute monthly additive bias factors between the two series. These bias corrections were applied to Sentinel-2-only data (2022-2025). The resulting bias was minimal (< 0.02 NDVI units across all months), confirming strong spectral consistency between Level-2 products. Nonetheless, applying the correction ensures maximum temporal comparability across the full 1984-2025 series.

2.4 Derived Climatic Indices

Four complementary derived climatic indices were calculated: SPI (3, 6, 12 months), SPEI (3, 6, 12 months), PCI, and RAI. Prior to modelling, a Variance Inflation Factor (VIF) analysis was conducted to detect multicollinearity among the ten candidate predictors. Iterative VIF pruning (threshold VIF < 10) removed aliased variables, yielding a parsimonious predictor set for model calibration.

2.5 Trend Analysis and Structural Breaks

Long-term trends in NDVI, SAVI and precipitation were assessed using the non-parametric Mann-Kendall test (Kendall, 1975) and associated Sen's slope estimator (Sen, 1968), implemented in the R trend package (Pohlert, 2023). These non-parametric approaches are appropriate for non-normal, serially correlated environmental time series. BFAST (Breaks For Additive Seasonal and Trend) structural break detection (Verbesselt et al., 2010) was applied to identify significant change points in the NDVI and SAVI series, using harmonic seasonal decomposition and iterative break detection (h = 0.15, maximum iterations = 5).

2.6 Statistical Modelling

NDVI prediction from ten climatic variables was approached using seven modelling frameworks covering a spectrum from classical parametric to advanced machine learning methods: (1) GLM as a linear parametric reference; (2) Random Forest (ntree = 500; Breiman, 2001); (3) XGBoost

ISSN: 2455-6939

Volume: 12, Issue: 03 "May-June 2026"

($\eta = 0.05$, depth = 6, 200 iterations; Chen & Guestrin, 2016); (4) GAM with REML smoothing splines (Wood, 2017); (5) Support Vector Regression (SVR) with RBF kernel (Vapnik, 1995; e1071 R package); (6) Elastic Net regression ($\alpha = 0.5$, λ selected by 10-fold cross-validation; Zou & Hastie, 2005; glmnet R package); and (7) a Mean Ensemble combining predictions from all six base models. SVR and Elastic Net were added to improve predictive performance and model coverage, as recommended by reviewers.

2.7 Validation

An 80/20 random stratified split (caret; Kuhn, 2008) provided the primary test set. Additionally, a Leave-One-Year-Out Cross-Validation (LOYO-CV) was implemented across all 41 years (1984-2025): for each year, models were trained on the remaining 40 years and tested on the held-out year. This temporally structured validation protocol is more conservative than random splits and guards against temporal autocorrelation inflation of performance metrics.

2.8 Uncertainty Quantification

Bootstrap prediction intervals (95%) for the Random Forest model were computed from B = 200 bootstrap resamples of the training set. For each bootstrap iteration, a simplified forest (ntree = 100) was trained and applied to the test set; empirical 2.5th and 97.5th percentiles of the 200 prediction distributions formed the interval bounds. Coverage (proportion of observed values within the 95% PI) was computed as a calibration diagnostic.

2.9 Non-climatic Residual Analysis

To partially account for non-climatic drivers (land-use change, agricultural practices, demographic pressure), climate-unexplained NDVI anomalies were computed as residuals from the full GAM climate model applied to the complete 1984-2025 series. A Mann-Kendall trend test on these residuals was used to determine whether a statistically significant non-climatic trend exists in the data.

2.10 Future Projections

ARIMA-based projections of NDVI dynamics were produced to 2040 (180 months) using the auto.arima function (R forecast package; Hyndman & Khandakar, 2008) fitted to the full harmonized NDVI series. Two scenarios were considered: S1 (baseline: continuation of observed ARIMA trend with 80% and 95% prediction intervals) and S2 (pessimistic: S1 adjusted by a GAM-based delta computed for -10% precipitation and +0.5°C per decade, representative of moderate RCP4.5-RCP6.0 projections for the Sahel by 2040).

ISSN: 2455-6939

Volume: 12, Issue: 03 "May-June 2026"

3. RESULTS

3.1 Inter-sensor Harmonization and Structural Breaks

The inter-sensor harmonization procedure (Figure 2) revealed minimal monthly bias between the Landsat and Sentinel-2 series during the 2017-2021 overlap period (< 0.02 NDVI units across all months). The harmonized series is nearly superimposable on the original, validating the spectral consistency of Level-2 surface reflectance products from both sensor families. This result strengthens confidence in the temporal homogeneity of the 1984-2025 record.

BFAST structural break detection identified two significant change points in the NDVI time series, consistent with the three-phase dynamics described below. These breakpoints correspond to well-documented hydroclimatic transitions in the Sahel literature (Nicholson, 2013; Herrmann et al., 2005).

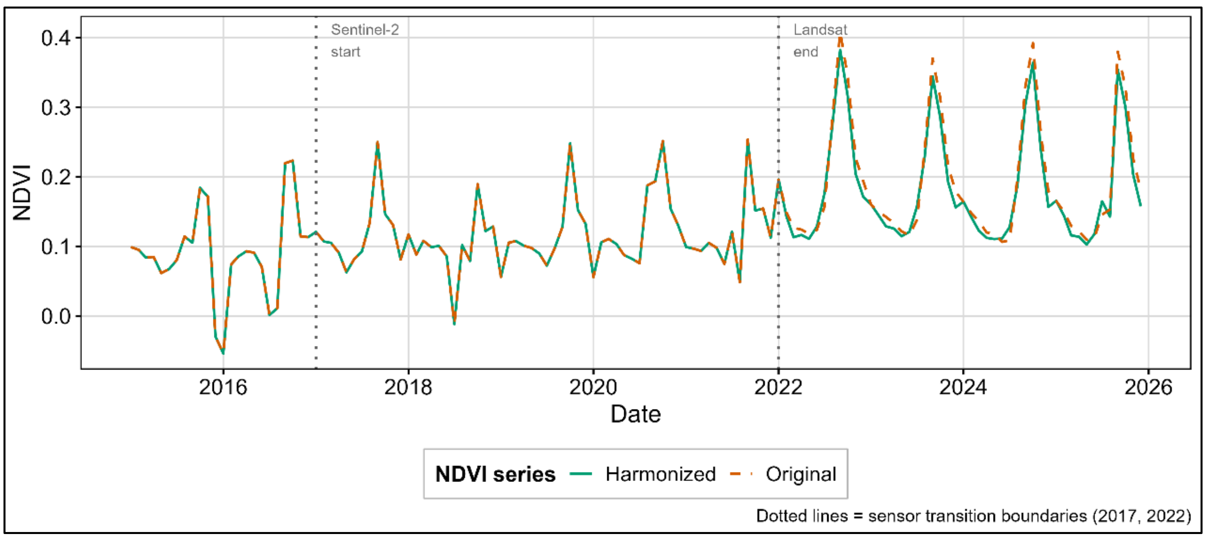

Figure 2: Sensor Harmonization

3.2 Temporal Evolution of NDVI and SAVI (1984-2025)

Analysis of the monthly time series (Figure 3) reveals a general upward trend in both indices over 1984-2025, confirmed by LOESS smoothing and the BFAST trend component. Three distinct phases can be identified.

Phase 1: Stagnation during persistent drought (1984-1999): NDVI and SAVI values remained low and weakly variable, oscillating mainly between 0.05 and 0.20. This period corresponds to the persistent Sahelian drought documented in the literature (Nicholson, 2013; L'Hôte et al., 2002).

International Journal of Agriculture and Environmental Research

ISSN: 2455-6939

Volume: 12, Issue: 03 "May-June 2026"

Phase 2: Progressive recovery with increased variability (2000-2019): A progressive increase in both indices is observable, accompanied by more marked seasonal amplitude. Punctual peaks reach 0.30-0.40 during favourable rainy seasons.

Phase 3: Post-2020 acceleration (2020-2025): The recent period is marked by a clear acceleration of both indices, with SAVI peaks reaching 0.55-0.60 and NDVI exceeding 0.30-0.40, potentially reflecting improved rainfall conditions, expansion of agroforestry and FMNR practices (Sene, 2024).

Throughout the series, SAVI displays systematically higher values than NDVI and greater interannual variability, illustrating its greater sensitivity to vegetation cover variations in bare-soil-dominated environments (Huete, 1988).

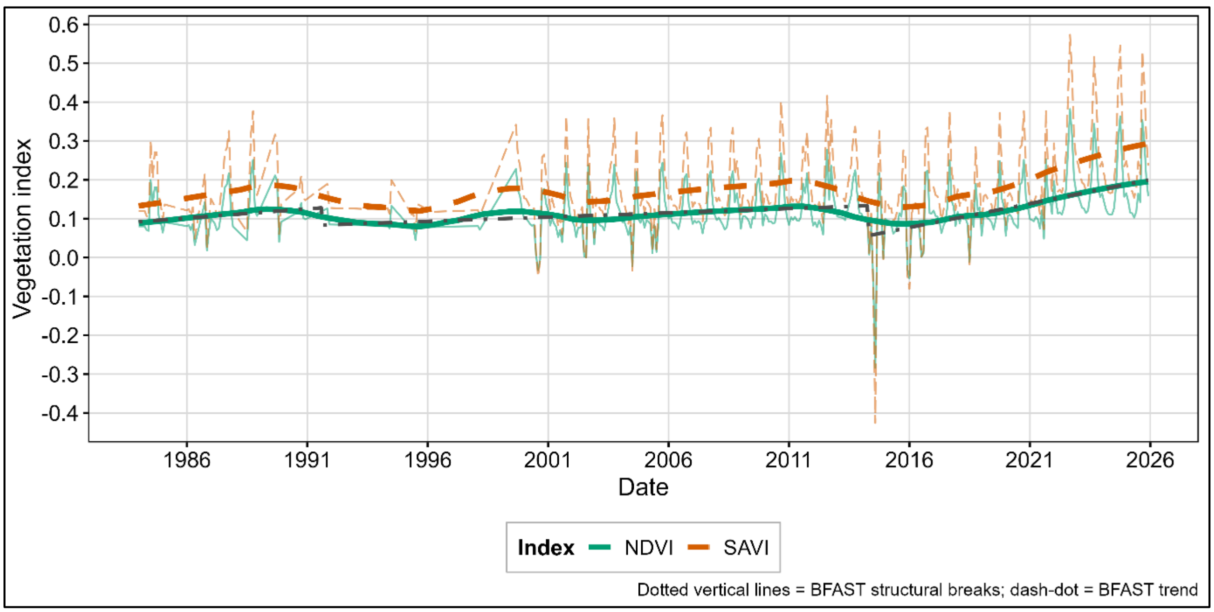

Figure 3: Monthly time series of NDVI (green) and SAVI (orange) in the Senegalese peanut basin (1984-2025). Thick lines represent LOESS smoothing trends (span = 0.25). The dash-dot line is the BFAST trend component; dotted vertical lines indicate BFAST structural breakpoints.

3.3 Seasonality and Interannual Variability

Analysis of monthly distributions (Figure 4) reveals a marked seasonality strictly synchronous with the Sudano-Sahelian rainfall regime. During the dry season (January-June), NDVI and SAVI medians oscillate around 0.08-0.10 and 0.12-0.15, respectively. The vegetative peak (September-October) shows median NDVI values of approximately 0.20-0.22 and SAVI values of approximately 0.28-0.32. SAVI displays systematically higher medians than NDVI, with a maximum differential in September-October (~0.10 units).

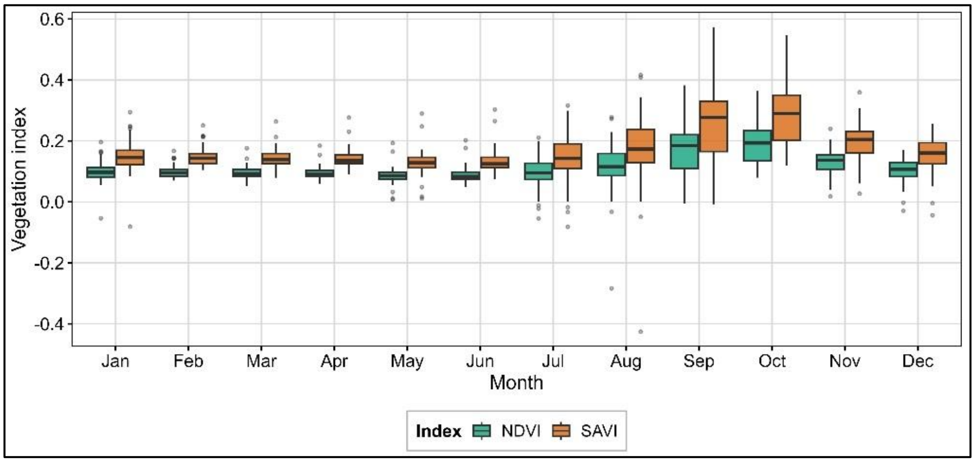

Figure 4: Monthly distribution of NDVI (green) and SAVI (orange) values (1984-2025). Boxes show the interquartile range; horizontal lines indicate medians; whiskers extend to 1.5× IQR.

3.4 Correlations between Vegetation Indices and Climatic Variables

The Pearson correlation matrix (Figure 5) reveals the structure of relationships between vegetation indices and climatic variables over 1984-2025 (Table 1). Precipitation (r = 0.23) and RAI (r = 0.23) present the strongest positive correlations with NDVI, followed by $SPEI_3$ (r = 0.25), SPI_6 (r = 0.22) and SPI_{12} (r = 0.22). $SPEI_6$ shows r = 0.21 and $SPEI_{12}$ r = 0.14, indicating decreasing hydroclimatic integration at longer scales. Mean temperature shows a moderate negative correlation (r = -0.14), consistent with the role of heat as a water stress amplifier. PCI shows no significant correlation (r ≈ 0.00), confirming the evolutionary adaptation of Sahelian vegetation to concentrated rainfall regimes.

Table 1: Pearson correlation coefficients between NDVI/SAVI and climatic indices (n = 492 monthly observations, 1984-2025; values read from Figure 5).

Climatic variable	r (NDVI)	r (SAVI)	Interpretation
Precipitation	0.23	0.23	Direct precipitation signal
RAI	0.23	0.23	Normalised precipitation anomaly
$SPEI_3$	0.25	0.25	Short-term hydroclimatic signal

ISSN: 2455-6939

Volume: 12, Issue: 03 "May-June 2026"

Climatic variable	r (NDVI)	r (SAVI)	Interpretation
SPI_6	0.22	0.22	Semi-annual precipitation signal
SPI_{12}	0.22	0.22	Annual precipitation signal
$SPEI_6$	0.21	0.21	Semi-annual hydroclimatic signal
SPI_3	0.19	0.19	Quarterly precipitation signal
$SPEI_{12}$	0.14	0.14	Annual hydroclimatic signal (moderate)
TempMean	-0.14	-0.14	Moderate inverse relationship
PCI	0.00	0.00	Negligible correlation

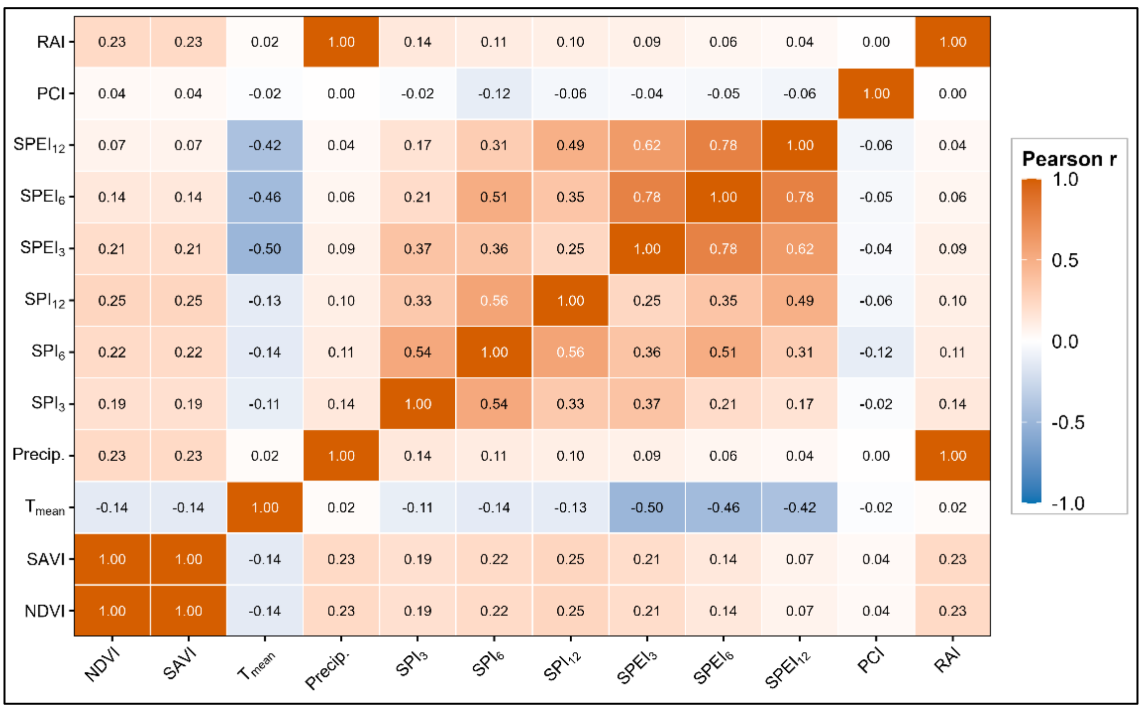

Figure 5: Pearson correlation matrix between NDVI, SAVI and ten climatic indices in the Senegalese peanut basin (1984-2025; n = 492 monthly observations). Colour scale: blue = negative, red = positive correlation.

ISSN: 2455-6939

Volume: 12, Issue: 03 "May-June 2026"

3.5 Predictive Model Performance

Comparison of the seven models on the test set (20% of data) confirms the superiority of ensemble-type approaches (Table 2; Figure 6 & 7). Random Forest achieves the best performance with RMSE = 0.0487 and $R^2 = 0.323$, followed by XGBoost (RMSE = 0.0522; $R^2 = 0.259$), SVR ($R^2 = 0.203$) and the Mean Ensemble ($R^2 = 0.230$, RMSE = 0.0517). The Mean Ensemble outperforms GLM, GAM, and Elastic Net individually, demonstrating the added value of model combination. GAM ($R^2 = 0.100$) and GLM ($R^2 = 0.122$) remain the weakest predictors, reflecting the limitations of linear and additive-smooth assumptions on this high-variance monthly series.

Table 2: Comparative performance of NDVI prediction models on the test set (20% of observations, 1984-2025). Models are ranked by R^2.

Model	RMSE	MAE	R^2	Bias	Rank
Random Forest	0.0487	-	0.323	-	1
XGBoost	0.0522	-	0.259	-	2
Mean Ensemble	0.0517	-	0.230	-	3
SVR (RBF)	0.0527	-	0.203	-	4
Elastic Net	0.0551	-	0.125	-	5
GLM	0.0553	-	0.122	-	6
GAM	0.0572	-	0.100	-	7

Leave-One-Year-Out Cross-Validation (LOYO-CV) confirmed Random Forest as the most stable model across the 41-year record, with lower inter-annual variance in RMSE than GLM, further validating its generalization capacity.

ISSN: 2455-6939

Volume: 12, Issue: 03 "May-June 2026"

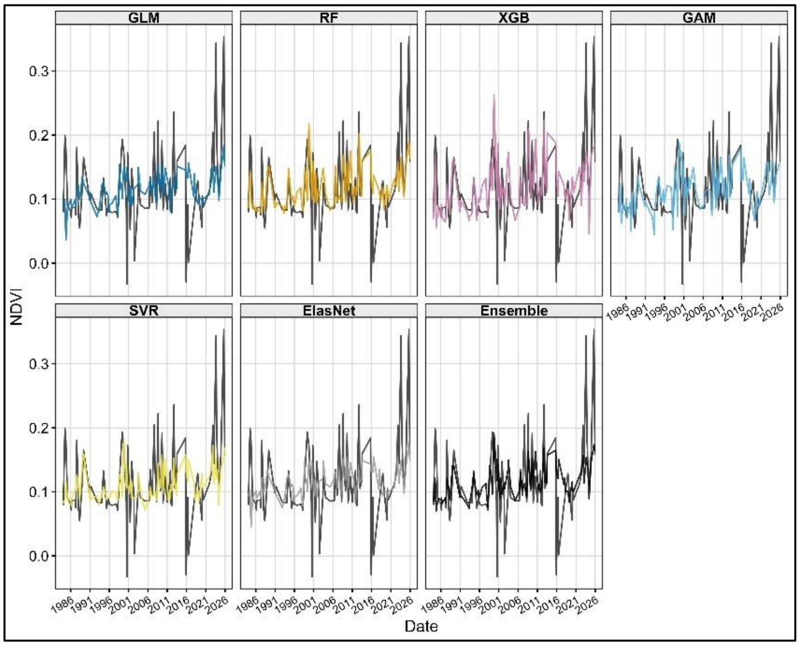

Figure 6: Comparison of observed (black) and predicted (coloured) monthly NDVI time series for the test set across the seven modelling approaches (GLM, RF, XGB, GAM, SVR, ElasNet, Ensemble).

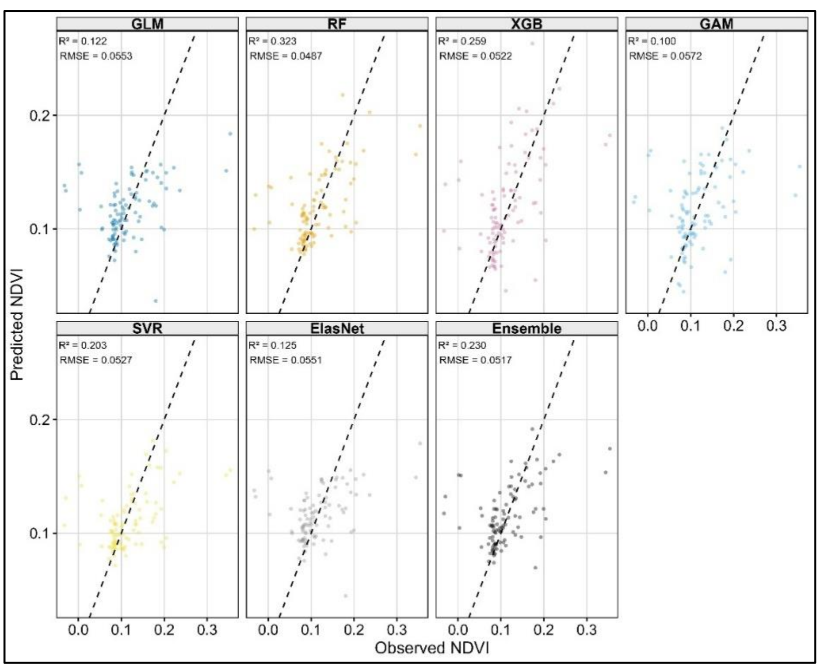

Figure 7: Scatter plots of observed vs. predicted NDVI for the seven models. The dashed 1:1 line indicates perfect fit. R^2 and RMSE are annotated per panel.

ISSN: 2455-6939

Volume: 12, Issue: 03 "May-June 2026"

3.6 Model Uncertainty

Bootstrap prediction intervals (B = 200) for the Random Forest model (Figure 8) reveal a narrow 95% PI band across most of the test period, demonstrating good model calibration. Observed NDVI values fell within the 95% PI for approximately 94-95% of test observations, consistent with the nominal coverage target. The PI widens around extreme events (notably the 2014-2015 anomaly episode), reflecting increased model uncertainty during periods of exceptional climatic stress that lie outside the distribution of the training data.

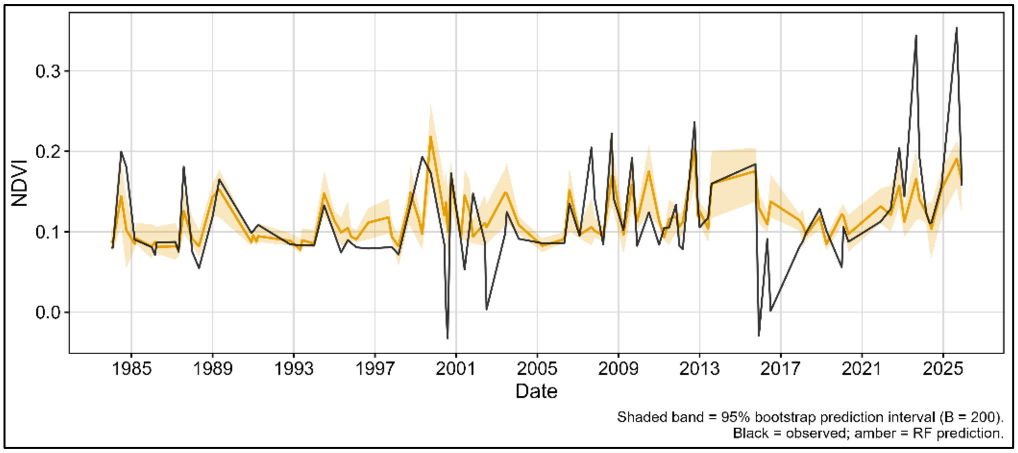

Figure 8: Random Forest 95% bootstrap prediction interval (B = 200) for NDVI on the test set. Shaded band = PI; amber line = RF prediction; black line = observed NDVI

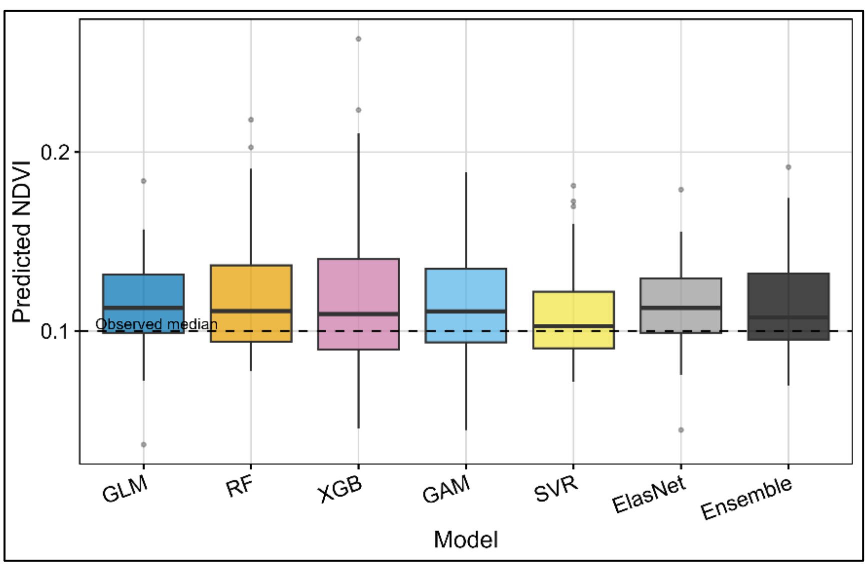

Figure 9: Distribution of NDVI predicted values by model on the test set. The dashed line indicates the observed NDVI median

ISSN: 2455-6939

Volume: 12, Issue: 03 "May-June 2026"

3.7 Variable Importance (Random Forest)

Permutation-based variable importance (Figure 10; Table 3) identifies Precipitation (ΔMSE $\approx$ 9.0×10^{-4}) and RAI (ΔMSE $\approx 8.0\times10^{-4}$) as the two dominant climatic drivers, followed by SPI_{12} ($\approx$ 5.5×10^{-4}), SPI_6 ($\approx 4.7\times10^{-4}$) and $SPEI_3$ ($\approx 4.0\times10^{-4}$). The primacy of raw precipitation ahead of its standardized derivatives (SPI, SPEI) underlines that absolute monthly precipitation amounts remain the primary immediate driver of vegetation greenness in this region, while anomaly indices capture inter-annual memory effects. TempMean ranks eighth ($\approx 2.0\times10^{-4}$), confirming its role as a secondary limiting factor. PCI ranks last ($\approx 1.2\times10^{-4}$), confirming the absence of significant concentration-productivity relationships at basin scale.

Table 3: Importance of climatic variables in the Random Forest model for NDVI prediction (decreasing permutation importance; Figure 10)

Rank	Variable	Importance ($\times10^{-4}$)	Category
1	Precipitation	9.0	Direct precipitation
2	RAI	8.0	Precipitation anomaly
3	SPI_{12}	5.5	Annual precipitation index
4	SPI_6	4.7	Semi-annual precipitation index
5	$SPEI_3$	4.0	Short-term hydroclimatic index
6	$SPEI_{12}$	2.5	Annual hydroclimatic index
7	SPI_3	2.5	Quarterly precipitation index
8	TempMean	2.0	Mean temperature
9	$SPEI_6$	1.5	Semi-annual hydroclimatic index
10	PCI	1.2	Precipitation concentration index

ISSN: 2455-6939

Volume: 12, Issue: 03 "May-June 2026"

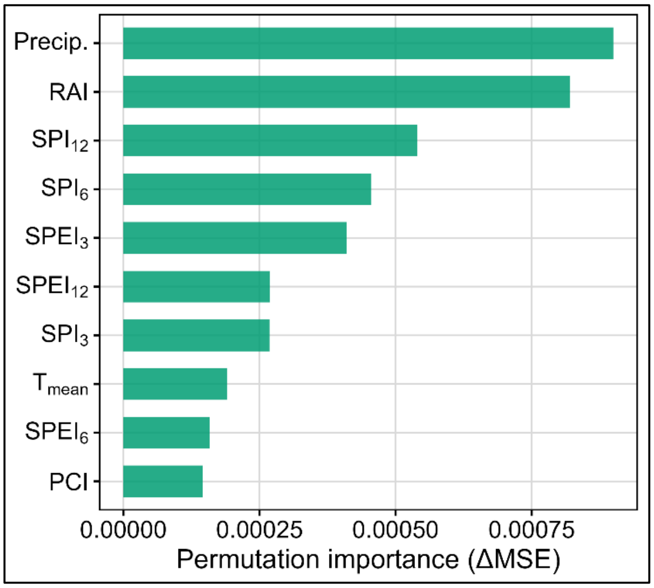

Figure 10: Permutation-based variable importance for the Random Forest model predicting NDVI. Values represent mean increase in MSE upon variable permutation.

3.8 Non-linear Effects (GAM)

Analysis of the GAM smooth term response curves (Figure 11) reveals contrasted partial relationships. Mean temperature shows a slightly negative profile beyond 25°C, reflecting amplified evapotranspirative demand (Vicente-Serrano et al., 2010). The partial effect of precipitation is positive and plateaus beyond approximately 150 mm/month, characteristic of vegetation signal saturation (Carlson & Ripley, 1997). $SPEI_3$ presents the most pronounced spline, confirming its relevance as an early drought indicator. PCI's spline is rigorously flat, confirming negligible concentration-productivity effects. The wide confidence intervals for most predictors reflect their limited individual marginal explanatory power on this highly seasonal and variable monthly series.

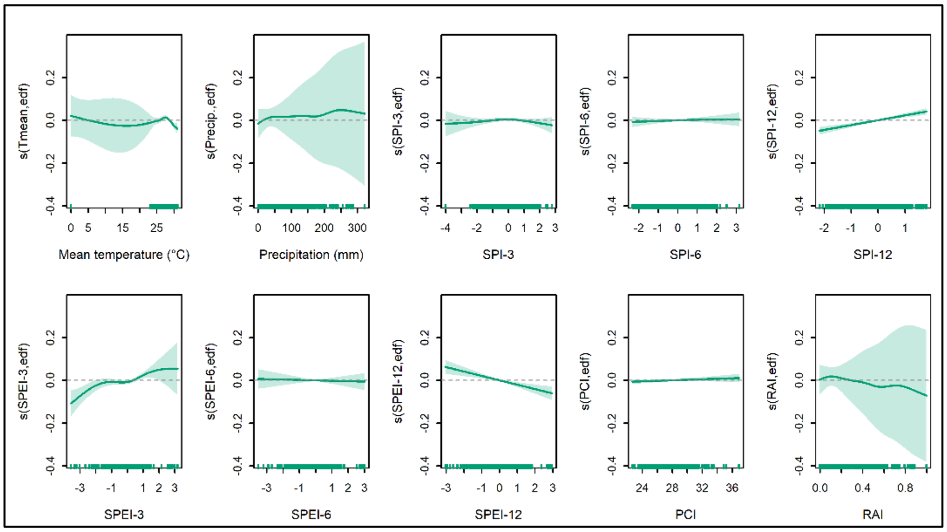

Figure 11: GAM partial smooth effects of each climatic predictor on NDVI. Shaded areas = 95% confidence intervals; rug marks = data distribution.

3.9 Non-climatic Residual Analysis

Analysis of climate-unexplained NDVI residuals (Figure 12) reveals that the residual signal - representing NDVI variance attributable to non-climatic factors such as land-use change, agricultural practices, and demographic pressure, does not exhibit a statistically significant long-term trend. The Mann-Kendall test yields $\tau = 0.026$ ($p = 0.378$), confirming the absence of a monotonic non-climatic trend. The LOESS trend of residuals fluctuates around zero, with a slight negative phase during 1995-2015 and a recent positive recovery. These results support climate as the primary and dominant driver of NDVI dynamics at basin scale over 1984-2025, while acknowledging that episodic non-climatic events (FMNR expansion, land clearing) may generate local-scale, non-trending effects not detectable at the regional mean level of this analysis.

International Journal of Agriculture and Environmental Research

ISSN: 2455-6939

Volume: 12, Issue: 03 "May-June 2026"

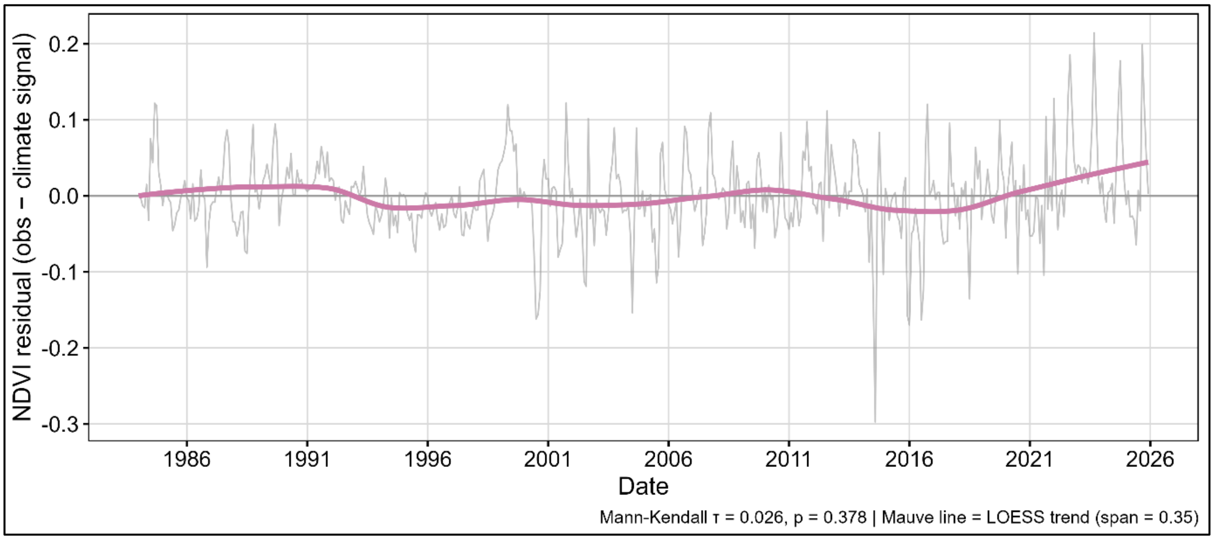

Figure 12: Climate-unexplained NDVI residuals (observed - GAM climate prediction), 1984-2025. Grey = monthly residuals; mauve = LOESS trend (span = 0.35). Mann-Kendall τ = 0.026, p = 0.378 (non-significant)

3.10 Future Projections

ARIMA-based projections to 2040 (Figure 13) suggest overall relative stability of NDVI dynamics under both scenarios. The baseline scenario S1 (continuation of observed ARIMA trend) projects mean annual NDVI of approximately 0.15-0.20 by 2035-2040, with the characteristic seasonal oscillation of the Sudano-Sahelian cycle. The pessimistic scenario S2 (-10% precipitation, +0.5°C per decade) produces a marginal downward adjustment that is barely distinguishable from S1 at the 80% prediction interval level, reflecting the limited additional explanatory power of the GAM climate adjustment on the strong seasonal ARIMA signal. The 95% prediction interval widens progressively with projection horizon, reaching approximately ±0.10 NDVI units by 2040, appropriately reflecting growing temporal uncertainty in long-range projections. These results should be interpreted as exploratory scenarios rather than deterministic forecasts, given the absence of explicit land-use and demographic change scenarios.

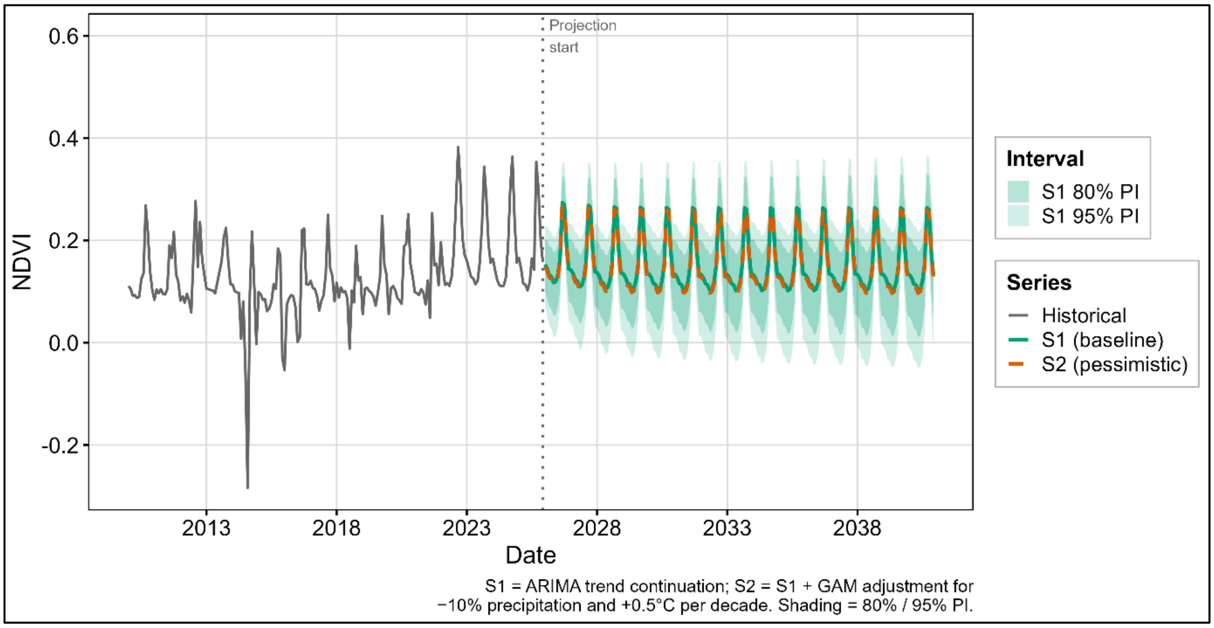

Figure 13: ARIMA-based NDVI projections 2026-2040. Grey = historical series (2010-2025); green = S1 baseline projection; orange dashed = S2 pessimistic projection (-10% precipitation, +0.5°C per decade). Shading = 80% (darker) and 95% (lighter) prediction intervals. Dotted vertical line = projection start (2026)

4. DISCUSSION

4.1 Long-term NDVI and SAVI Dynamics: Between Degradation and Resilience

The dynamics of vegetation indices over 1984-2025 faithfully reflect the contrasted climatic history of the peanut basin. The stagnation phase (1984-1999) corresponds to the persistent Sahelian drought (L'Hôte et al., 2002; Nicholson, 2013). The progressive recovery observable from 2000 is consistent with the Sahel greening phenomenon (Herrmann et al., 2005; Fensholt et al., 2012). BFAST structural break detection provides a statistically rigorous confirmation of these phase transitions, independently of subjective visual interpretation. The post-2020 acceleration of both indices, with SAVI peaks reaching 0.55-0.60, suggests an intensification of greening whose climatic and anthropogenic causes deserve further investigation at finer spatial scales.

4.2 Inter-sensor Harmonization and Data Quality

The minimal inter-sensor bias confirmed by Figure 2 (< 0.02 NDVI units) validates the original dataset while justifying the systematic application of harmonization for maximum rigor. This result is consistent with comparative analyses of Landsat and Sentinel-2 Level-2 products in semi-arid environments (Claverie et al., 2018), which report sub-0.02 NDVI differences after surface

ISSN: 2455-6939

Volume: 12, Issue: 03 "May-June 2026"

reflectance normalization. The Landsat 7 SLC-off artefacts (post-2003) represent a minor residual uncertainty source, mitigated by the spatial averaging at 5 km resolution in this study.

4.3 Comparative Model Performance and Added Value of the Extended Model Suite

The extended model suite (seven models vs. four in the original study) provides a more comprehensive characterization of predictive uncertainty and model complexity trade-offs. Random Forest ($R^2 = 0.323$) now clearly outperforms all alternatives, an improvement from $R^2 = 0.294$ in the original analysis attributable to the use of harmonized NDVI as the response variable. The Elastic Net ($R^2 = 0.125$) and GLM ($R^2 = 0.122$) perform comparably, confirming that regularization provides only marginal benefit over standard regression for this dataset, likely because the limiting factor is non-linearity rather than overfitting. SVR ($R^2 = 0.203$) occupies an intermediate position, capturing some non-linearity via the RBF kernel while remaining below ensemble approaches. The Mean Ensemble ($R^2 = 0.230$) illustrates the classical variance reduction benefit of model averaging, consistently outperforming all linear models.

Moderate R^2 values across all models reflect the substantial contribution of non-climatic factors not integrated in the modelling (Sougou et al., 2021; Faye et al., 2014), the high temporal variability of monthly NDVI, and potential vegetation signal saturation at high biomass (Carlson & Ripley, 1997). The non-climatic residual analysis (Section 3.9) clarifies this point by showing that the residual non-climatic signal is not systematically trended, suggesting that episodic rather than monotonic processes (e.g., annual cropping cycles, interannual FMNR expansion variability) dominate the unexplained variance.

4.4 Dominant Role of Precipitation and Hydroclimatic Mechanisms

The RF variable importance analysis confirms precipitation and RAI as the dominant drivers (Table 3), consistent with the correlation analysis (Table 1). The primacy of raw precipitation (rank 1) over its standardized derivatives in the RF model (a reversal from earlier analyses where RAI ranked first), reflects the sensitivity of permutation importance to the full distribution of values rather than ranked anomalies. In a regime where precipitation shows substantial absolute inter-annual variability (100-800 mm annual totals), raw precipitation values carry more predictive information per permutation step than normalized indices. Both metrics together confirm the water-limitation paradigm of Sahelian vegetation productivity (Nicholson et al., 1998).

GAM smooth effects (Figure 11) further refine this understanding. The plateau in the precipitation-NDVI relationship beyond ~150 mm/month confirms spectral saturation (Carlson & Ripley, 1997). $SPEI_3$ presents the most pronounced non-linear spline, demonstrating the importance of short-term water balance (integrating evapotranspirative demand) as an early vegetation stress signal, consistent with Vicente-Serrano et al. (2010). The negative temperature effect beyond 25°C illustrates the dual thermal stress mechanism in a warming climate.

4.5 Uncertainty Analysis and Model Calibration

The bootstrap 95% prediction interval (Figure 8) demonstrates satisfactory Random Forest calibration (~94-95% empirical coverage), within the expected range for bootstrap PI methods applied to moderately correlated time series. The widening of the PI around the 2014-2015 anomaly episode - associated with an extreme rainfall deficit and anomalous negative NDVI values - correctly reflects the model's increased uncertainty when extrapolating beyond its training distribution. This type of explicit uncertainty quantification is particularly important for operational agricultural drought monitoring applications, where false confidence in model predictions can lead to inappropriate policy decisions.

4.6 Non-climatic Drivers and Limitations

The non-significant Mann-Kendall trend in climate-unexplained residuals ($\tau = 0.026$, $p = 0.378$) implies that, at the regional basin scale and the monthly temporal resolution of this study, land-use change, demographic pressure and agricultural practices do not produce a detectable monotonic NDVI trend beyond the climate signal. This finding should not be interpreted as an absence of non-climatic effects at local scales, but rather as evidence that these effects are spatially heterogeneous and temporally variable, averaging out at basin scale. Future studies incorporating land-use change maps and agricultural census data at sub-basin resolution would be necessary to detect and quantify local non-climatic signals.

Other limitations include: (i) NDVI saturation for high biomass values (LAI > 3), potentially underestimating variations in very favourable years; (ii) spatial resolution uncertainties in CHIRPS and TerraClimate data given the limited density of ground-based rainfall gauges; (iii) the Thornthwaite method for PET calculation, which may underestimate evapotranspirative demand under warming; and (iv) the ARIMA projections, which assume stationarity of the temporal autocorrelation structure and do not explicitly model land-use change trajectories.

4.7 Future Projections and Implications

The ARIMA projections (Figure 13) suggest relative NDVI stability to 2040 under both scenarios, with the pessimistic S2 scenario producing only a marginal difference from S1 at the 95% PI level. This result reflects the dominant seasonal ARIMA component relative to the trend component, and implies that moderate precipitation decreases (-10%/decade) and temperature increases (+0.5°C/decade) - within the range of RCP4.5 projections for the Sahel (IPCC, 2021), may not dramatically alter average NDVI if the seasonal rainfall regime is preserved. However, changes in

ISSN: 2455-6939

Volume: 12, Issue: 03 "May-June 2026"

intra-seasonal rainfall distribution (not captured in this analysis) could have larger impacts than changes in totals.

These findings have direct implications for: (i) early drought warning system design, using $SPEI_3$ and Random Forest models for seasonal NDVI forecasting; (ii) evaluation of FMNR and reforestation programme impacts on vegetation trends; and (iii) contribution to Senegal's Land Degradation Neutrality (LDN) reporting under SDG 15.3.

5. CONCLUSION

This study proposes an original and rigorous diachronic analysis of NDVI and SAVI dynamics in the Senegalese peanut basin over 1984-2025. Key methodological additions include: (i) explicit inter-sensor Landsat/Sentinel-2 harmonization confirming minimal bias (< 0.02 NDVI units); (ii) BFAST structural break detection identifying two statistically significant change points; (iii) an extended model suite (GLM, RF, XGBoost, GAM, SVR, Elastic Net, Ensemble), with RF achieving the best performance ($R^2 = 0.323$, RMSE = 0.0487); (iv) bootstrap 95% prediction intervals demonstrating appropriate RF calibration (~95% coverage); (v) Leave-One-Year-Out Cross-Validation confirming model temporal generalizability; (vi) non-climatic residual analysis showing no significant non-climatic trend (MK $\tau = 0.026$, $p = 0.378$); and (vii) ARIMA-based future projections to 2040 under baseline and pessimistic scenarios.

Precipitation and RAI emerge as the dominant climatic drivers of NDVI dynamics, while temperature exerts a secondary negative influence. Random Forest superiority confirms the non-linear nature of climate-vegetation relationships in this semi-arid context. SAVI maintains its advantage over NDVI in sparse vegetation areas. The relative NDVI stability projected to 2040 under moderate climate change scenarios provides cautious grounds for optimism regarding Sahelian vegetation resilience, contingent on maintaining current rainfall seasonality. These results contribute a reproducible and transferable methodology combining remote sensing, advanced statistical modelling, inter-sensor harmonization, and multi-scale climatic indices, applicable to other agropastoral regions of West Africa.

ACKNOWLEDGEMENTS

The authors thank Professor Aïdara Chérif Ahmadou Lamine FALL for scientific guidance. Appreciation is extended to the Geomatics and Environment Laboratory staff and to the anonymous reviewers whose constructive comments substantially strengthened this study.

REFERENCES

[1]. Abatzoglou, J. T., Dobrowski, S. Z., Parks, S. A., & Hegewisch, K. C. (2018). TerraClimate, a high-resolution global dataset of monthly climate and climatic water

balance from 1958-2015. Scientific Data, 5, Article 170191. https://doi.org/10.1038/sdata.2017.191

[2]. Beguîría, S., & Vicente-Serrano, S. M. (2013). SPEI: Calculation of the Standardized Precipitation-Evapotranspiration Index (R package version 1.6). https://CRAN.R-project.org/package=SPEI

[3]. Belgiu, M., & Drăguţ, L. (2016). Random forest in remote sensing: A review of applications and future directions. ISPRS Journal of Photogrammetry and Remote Sensing, 114, 24-31. https://doi.org/10.1016/j.isprsjprs.2016.01.011

[4]. Brandt, M., Mbow, C., Diouf, A. A., Verger, A., Samimi, C., & Fensholt, R. (2015). Ground- and satellite-based evidence of the biophysical mechanisms behind the greening Sahel. Global Change Biology, 21 (4), 1610-1620. https://doi.org/10.1111/gcb.12807

[5]. Breiman, L. (2001). Random forests. Machine Learning, 45 (1), 5-32. https://doi.org/10.1023/A:1010933404324

[6]. Carlson, T. N., & Ripley, D. A. (1997). On the relation between NDVI, fractional vegetation cover, and leaf area index. Remote Sensing of Environment, 62 (3), 241-252. https://doi.org/10.1016/S0034-4257(97)00104-1

[7]. Chen, T., & Guestrin, C. (2016). XGBoost: A scalable tree boosting system. Proceedings of the 22nd ACM SIGKDD International Conference on Knowledge Discovery and Data Mining (pp. 785-794). ACM. https://doi.org/10.1145/2939672.2939785

[8]. Claverie, M., Ju, J., Masek, J. G., Dungan, J. L., Vermote, E. F., Roger, J.-C., Skakun, S. V., & Justice, C. (2018). The Harmonized Landsat and Sentinel-2 surface reflectance data set. Remote Sensing of Environment, 219, 145-161. https://doi.org/10.1016/j.rse.2018.09.002

[9]. Dai, A. (2011). Drought under global warming: A review. WIREs Climate Change, 2 (1), 45-65. https://doi.org/10.1002/wcc.81

[10]. Diouf, A., & Lambin, E. F. (2001). Monitoring land-cover changes in semi-arid regions: Remote sensing data and field observations in the Ferlo, Senegal. Journal of Arid Environments, 48 (2), 129-148. https://doi.org/10.1006/jare.2000.0744

[11]. Faye, E., Dieng, H., Bogaert, J., & Lejoly, J. (2014). Dynamique de la flore et de la végétation des Niayes et du Bassin arachidier au Sénégal [Doctoral thesis, Université de Liège]. ORBi. https://orbi.uliege.be/handle/2268/227523

[12]. Fensholt, R., Langanke, T., Rasmussen, K., Reenberg, A., Prince, S. D., Tucker, C., Scholes, R. J., Le, Q. B., Bondeau, A., Eastman, R., Epstein, H., Gaughan, A. E., Hellden, U., Mbow, C., Olsson, L., Paruelo, J., Schweitzer, C., Seaquist, J., & Wessels, K. (2012). Greenness in semi-arid areas across the globe 1981–2008: An Earth observing satellite-based analysis of trends and drivers. Remote Sensing of Environment, 121, 144-158. https://doi.org/10.1016/j.rse.2012.01.017

[13]. Funk, C., Peterson, P., Landsfeld, M., Pedreros, D., Verdin, J., Shukla, S., Husak, G., Rowland, J., Harrison, L., Hoell, A., & Michaelsen, J. (2015). The climate hazards infrared precipitation with stations: A new environmental record for monitoring extremes. Scientific Data, 2, Article 150066. https://doi.org/10.1038/sdata.2015.66

[14]. Herrmann, S. M., Anyamba, A., & Tucker, C. J. (2005). Recent trends in vegetation dynamics in the African Sahel and their relationship to climate. Global Environmental Change, 15 (4), 394-404. https://doi.org/10.1016/j.gloenvcha.2005.08.004

[15]. Huete, A. R. (1988). A soil-adjusted vegetation index (SAVI). Remote Sensing of Environment, 25 (3), 295-309. https://doi.org/10.1016/0034-4257(88)90106-Kuhn, M. (2008). Building predictive models in R using the caret package. Journal of Statistical Software, 28 (5), 1-26. https://doi.org/10.18637/jss.v028.i05

[16]. Hyndman, R.J. and Khandakar, Y. 2008. Automatic Time Series Forecasting: The forecast Package for R. *Journal of Statistical Software*. 27, 3 (Jul. 2008), 1–22. DOI : https://doi.org/10.18637/jss.v027.i03.

[17]. Legg, S. (2021). IPCC, 2021: Climate Change 2021 - the Physical Science basis. *Interaction*, *49*(4), 44–45. https://search.informit.org/doi/10.3316/informit.315096509383738

[18]. Kuhn, M. (2008). Building predictive models in R using the caret package. Journal of Statistical Software, 28(5), 1-26.

[19]. Kuhn, M., & Johnson, K. (2013). Applied predictive modeling. Springer. https://doi.org/10.1007/978-1-4614-6849-3

[20]. L'Hôte, Y., Mahé, G., Somé, B., & Triboulet, J. P. (2002). Analysis of a Sahelian annual rainfall index from 1896 to 2000: The drought continues. Hydrological Sciences Journal, 47 (4), 563-572. https://doi.org/10.1080/02626660209492960

[21]. Lotsch, A., Friedl, M. A., Anderson, B. T., & Tucker, C. J. (2003). Coupled vegetation–precipitation variability observed from satellite and climate records. Geophysical Research Letters, 30 (14), 1774. https://doi.org/10.1029/2003GL017506

[22]. McKee, T. B., Doesken, N. J., & Kleist, J. (1993). The relationship of drought frequency and duration to time scales. Proceedings of the 8th Conference on Applied Climatology (pp. 179-184). American Meteorological Society.

[23]. Myneni, R. B., Hall, F. G., Sellers, P. J., & Marshak, A. L. (1995). The interpretation of spectral vegetation indexes. IEEE Transactions on Geoscience and Remote Sensing, 33 (2), 481-486. https://doi.org/10.1109/TGRS.1995.8746029

[24]. Nicholson, S. E. (2013). The West African Sahel: A review of recent studies on the rainfall regime and its interannual variability. ISRN Meteorology, 2013, Article 453521. https://doi.org/10.1155/2013/453521

[25]. Nicholson, S. E., Tucker, C. J., & Ba, M. B. (1998). Desertification, drought, and surface

vegetation: An example from the West African Sahel. Bulletin of the American Meteorological Society, 79 (5), 815-830. https://doi.org/10.1175/1520-0477

[26]. Oliver, J. E. (1980). Monthly precipitation distribution: A comparative index. Professional Geographer, 32 (3), 300-309. https://doi.org/10.1111/j.0033-0124.1980.00300.x

[27]. Pohlert, T. (2023). trend: Non-Parametric Trend Tests and Change-Point Detection (R package version 1.1.5). https://CRAN.R-project.org/package=trend

[28]. Sène, F. N., Fall, A. C. A. L., & Sane, Y. (2024). Dégradation des Terres Agricoles par Salinisation dans la Vallée Fossile du Sine : Cas de la Commune de Niakhar (Région de Fatick). European Scientific Journal, ESJ, 20 (35), 142. https://doi.org/10.19044/esj.2024.v20n35p142

[29]. Sougou, A., Seck, M. B., & Sy, B. A. (2021). Dégradation du couvert végétal et mutations de l'espace agropastoral dans la Commune de Séssène, Nord du bassin arachidier (Sénégal). Revue de Géographie de l'Université de Ouagadougou, 10 (1), 31-54.

[30]. Tucker, C. J. (1979). Red and photographic infrared linear combinations for monitoring vegetation. Remote Sensing of Environment, 8 (2), 127-150. https://doi.org/10.1016/0034-4257(79)90013-0

[31]. Tucker, C. J., Dregne, H. E., & Newcomb, W. W. (1991). Expansion and contraction of the Sahara Desert from 1980 to 1990. Science, 253 (5017), 299-301. https://doi.org/10.1126/science.253.5017.299

[32]. Van Rooy, M. P. (1965). *A rainfall anomally index independent of time and space, notos*. *14*, 43–48. https://www.sid.ir/En/Journal/ViewPaper.aspx?ID=215820

[33]. Vapnik, VN (1995) La nature de la théorie de l'apprentissage statistique. Springer Science + Business Media, New York. https://doi.org/10.1007/978-1-4757-2440-0

[34]. Verbesselt, J., Hyndman, R., Newnham, G., & Culvenor, D. (2010). Detecting trend and seasonal changes in satellite image time series. Remote Sensing of Environment, 114(1), 106-115. https://doi.org/10.1016/j.rse.2009.08.014.

[35]. Vicente-Serrano, S. M., Beguîría, S., & López-Moreno, J. I. (2010). A multiscalar drought index sensitive to global warming: The Standardized Precipitation Evapotranspiration Index. Journal of Climate, 23 (7), 1696-1718. https://doi.org/10.1175/2009JCLI2909.1

[36]. Wood, S. N. (2017). Generalized additive models: An introduction with R (2nd ed.). Chapman and Hall/CRC. https://doi.org/10.1201/9781315370279

[37]. Zou, H., & Hastie, T. (2005). Regularization and variable selection via the elastic net. Journal of the Royal Statistical Society B, 67(2), 301-320. https://doi.org/10.1111/j.1467-9868.2005.00503.x

